



HAL
open science

Tethered Drone-Based Airborne Wind Energy System Launching and Retrieving

Audrey Schanen, Jonathan Dumon, Nacim Meslem, Ahmad Hably, Amaury
Nègre, Alexandre Sarazin

► **To cite this version:**

Audrey Schanen, Jonathan Dumon, Nacim Meslem, Ahmad Hably, Amaury Nègre, et al.. Tethered Drone-Based Airborne Wind Energy System Launching and Retrieving. *Journal of Guidance, Control, and Dynamics*, 2021, 44 (12), pp.2284. 10.2514/1.G006099 . hal-03328323

HAL Id: hal-03328323

<https://hal.science/hal-03328323>

Submitted on 27 Jul 2022

HAL is a multi-disciplinary open access archive for the deposit and dissemination of scientific research documents, whether they are published or not. The documents may come from teaching and research institutions in France or abroad, or from public or private research centers.

L'archive ouverte pluridisciplinaire **HAL**, est destinée au dépôt et à la diffusion de documents scientifiques de niveau recherche, publiés ou non, émanant des établissements d'enseignement et de recherche français ou étrangers, des laboratoires publics ou privés.

Tethered drone-based Airborne wind energy system launching and retrieving

Audrey Schanen ^{*}, Jonathan Dumon [†], Nacim Meslem [‡], Ahmad Hably [§], Amaury Nègre[¶], Alexandre Sarazin^{||}
Univ. Grenoble Alpes, CNRS, Grenoble INP^{}, GIPSA-Lab,
F-38000 Grenoble, France.*
^{}Institute of Engineering Univ. Grenoble Alpes*

I. Introduction

The French energy transition law imposes a reduction of the fossil energies down to 50% within 10 years. Transition scenarios foresees renewable part of energy production to reach between 40% and 70%, with an increasing portion of wind energy. By 2027, the IEA predicts that wind will be the number-one source of the EU's energy, but even that will not be enough to meet stringent emissions targets. Considering for example the floating offshore wind turbines, the material amount per unit of power involved in the construction of wind turbines and floating devices may render this concept unsustainable if it is scaled with current fossils energy production levels.

The emerging airborne wind energy (AWE) sector offers breakthrough concepts that will allow diversifying the wind energy production offer. The physics behind airborne wind energy includes diverse range of concepts involving aerodynamic tethered structures that capture high-altitude wind energy, of different power range (from KW to MW), and deliver it to the ground. As an example, Enerkite announces a system rated power of 500 kW for a wing area of $125m^2$ ^{*}. Other examples can be found in the review paper [1]. There are two main ways to categorize most airborne wind energy designs: soft-wing versus rigid-wing. In addition to those that generate energy in the air (on-board) versus those that use a pumping motion to power an on-ground generator (Fig. 1), [2].

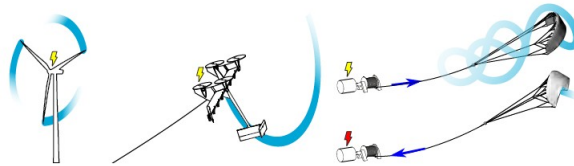


Fig. 1 From classical wind turbines to on-board and on-ground airborne wind energy systems, figure from [2].

Recent research results are gradually assessing and eliminating feasibility risks and improving the understanding of AWE systems. A key premise for airborne wind is that it should be able to significantly reduce costs by cutting the

^{*}PhD Student, GIPSA-Lab, audrey.schanen@gipsa-lab.fr

[†]Research engineer, GIPSA-Lab, CNRS, jonathan.dumon@gipsa-lab.fr

[‡]Associate professor, GIPSA-Lab, Grenoble-INP, nacim.meslem@grenoble-inp.fr

[§]Professor, GIPSA-Lab, Grenoble-INP, corresponding author, ahmad.hably@grenoble-inp.fr

[¶]Research engineer, GIPSA-Lab, CNRS, amaury.negre@gipsa-lab.fr

^{||}Engineer, GIPSA-Lab, alexandre.sarazin@gipsa-lab.fr

^{*}<https://www.enerkite.de/en/products.html>

amount of materials required for each generation unit, compared to traditional turbines. On the other hand, and unlike turbines, AWE systems have to cope with partially unpredictable wind to remain airborne and need to land when wind conditions are poor. Landings and launches are hard to automate, and each one raises the risk of catastrophic failure. Indeed, the presence of atmospheric turbulence in the lower layers of the atmospheric boundary layer as well as possibly the movement of the landing platform make the wind conditions very delicate (high turbulence and significant speed gradients). For example, in 2019, Makani's offshore 600kW energy kite prototype was lost during landing.

To remedy these issues, different solutions have been proposed. A control-based approach to a rotational take-off of an AWE system has been studied in [3]. In the Airborne Wind Energy Conference (AWEC 2017), three solutions for launching and landing of an EnerKite wing have been presented [4]: Vertical take-off, catapult, and rotating arm. Different concepts are analyzed theoretically in [5] for the take-off phase of AWE systems based on rigid wings and on-ground power conversion. A deeper numerical simulation of a linear take-off maneuver combined with on-board propellers has been also studied. The limitation of this maneuver is that it cannot handle neither the landing phase nor the impacts of the ground station design. For flexible wing/kite AWE systems, strategies such as static mast-based launch and landing are proposed by Skysails[†] or a rotating arm concept is explored in the Kitegen project [6]. The problem of automatically retracting the wing of an AWE system during the reel-in phase has been addressed in [7]. In relation to the present paper, in [8], static and dynamic feasibility analysis of using multicopter for autonomously launching and landing kites have been carried out. The authors pointed out a disadvantage in this solution for soft kites that is the kite generates a lift force opposite to the propeller thrust of the multicopter during the hovering phase. To remedy this problem, in a recent work [9], a vertical take-off strategy, using a multicopter, of a flexible kite AWE system have been studied in a simulation environment. The landing of the kite is done by the winch of the on-ground station without the multicopter assistance. In [10] a theoretical study on the take-off and landing phases of an AWE system composed by a rigid-wing and a multicopter has been presented. In this study, the motion of the AWE system is assumed inside a plane (2D) and the effectiveness of the proposed control law is assessed only in a simulation framework. In the present work, the former theoretical result in [10] is extended and completed to deal with an experimental test-bench. The novelties of this contribution can be summed up in the following three points: (i) a 3D space control law is proposed to steer a prototype AWE system; (ii) all the subsystems involved in the global control loop are introduced and discussions about their tuning parameters are presented; (iii) several experiments are performed to show the efficiency of the proposed control method on a lab test-bench.

The remainder of this paper is organized as follows. The objectives of this work are detailed in Section II as well as the modelling phases. In Section III, the considered control design approach is presented: first for the 2D case (plane) and then extended to the 3D case (space). Moreover, this section contains a detailed description of the used test-bench. The obtained experimental results are shown and discussed in Section IV. The paper ends by a conclusion and some

[†]<https://skysails-group.com/index.html>

perspectives presented in Section V.

II. Problem Statement

A. Objectives

In order to safely perform the take-off and landing phases of a drone-based AWE system, the objective is to steer it to a desired location (or position) in the air while maintaining the tether to a defined range of tension. To achieve that, a nonlinear multi-objectives controller is proposed to control simultaneously the drone and the on-ground winch. Since the main goal is to reach a target position and not to follow up closely a user-defined trajectory, a margin on the tracking error is tolerated while the system stays in a safety zone to avoid crashes. During the take-off and landing

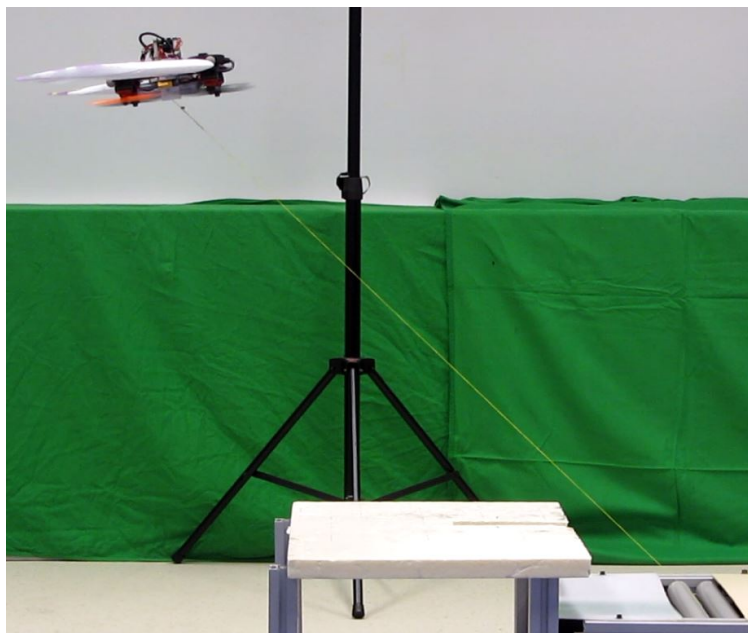


Fig. 2 In-flight drone-based airborne wind energy small scale prototype

phases, the best configuration corresponds to the system aligned in the wind direction. Knowing that, the modelling and the design of control laws for the tether length, elevation angle and tether tension can be done in the plane (2D). For the last variable, the azimuth angle, a similar control law as that applied to the elevation angle can be used. The azimuth angle in this case is decoupled from the rest of the system. The hypothesis is acceptable since the variations of the azimuth angle for this type of system are negligible.

B. System Modelling

As mentioned in the introduction, the airborne wind energy (AWE) system studied in this present paper is composed of two components: The first one is a flying device composed of a rigid wing with a multicopter or a drone and the second is an on-ground station. Both elements are connected by the means of a tether. In presence of wind, the flying

device generates aerodynamic lift and drag forces. For on-ground AWE systems, the resultant traction force is transferred via the tether to an on-ground generator where a drum is used to convert the linear motion of the tether into shaft power, that is then used to drive a generator. A thrust force is generated by the drone attached to the flying device in order to control the trajectory of the system, especially in absence of wind. The different forces related to the drone that act on the system are considered as introduced in [11]

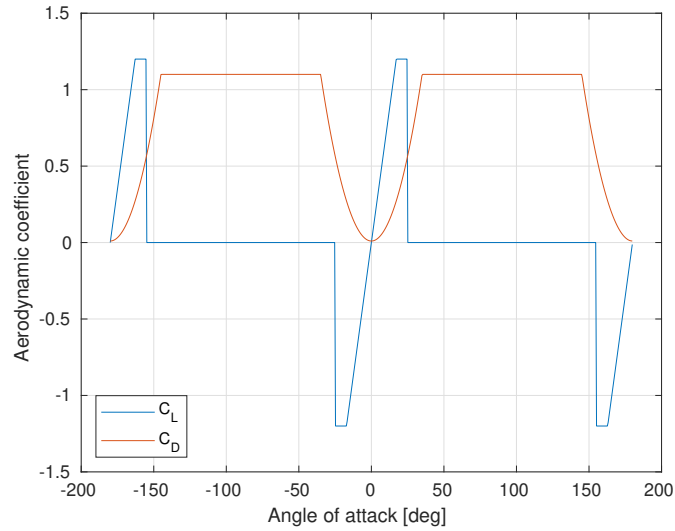


Fig. 3 Aerodynamic coefficient C_L and C_D in function of the wing’s angle of attack.

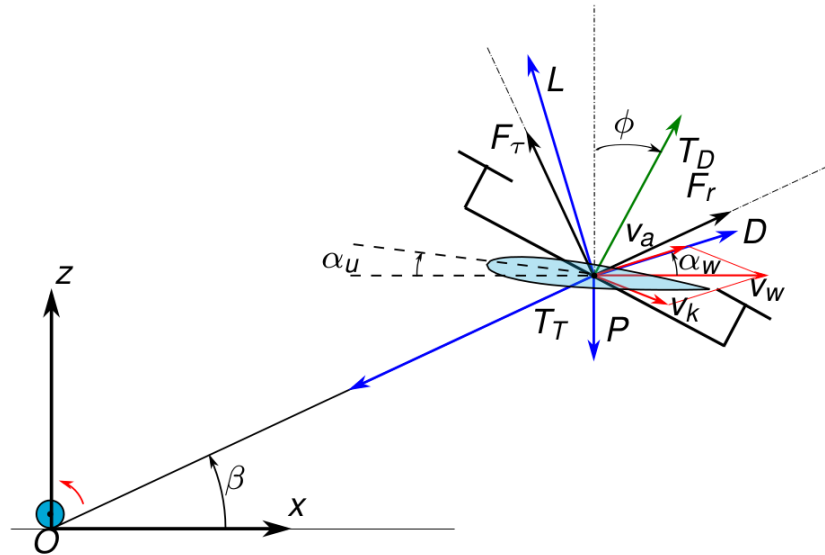


Fig. 4 The airborne wind energy system with the drone connected to the on-ground station. All forces acting on the system are shown.

In order to establish the model, all the forces acting on the system have to be expressed. We will consider all the

aerodynamic forces generated by the wing in presence of wind. These forces depend on the aerodynamic properties of the wing and its profile. The lift and drag forces can be expressed by:

$$L = \frac{1}{2}\rho S v_a^2 C_L, \quad D = \frac{1}{2}\rho S v_a^2 C_D \quad (1)$$

where ρ is the air density, v_a is the apparent wind velocity, S is the considered wing surface, C_L and C_D are respectively aerodynamic lift and drag coefficients. In order to determine them, one can refer to the aerodynamic coefficient curves of Fig. 3, generated from the equations of [12].

Figure 4 gives a general overview of the considered system, with all forces acting on the system represented as the aerodynamic forces, L and D , the weight P , the tether tension T_T and the thrust of the drone T_D . As it is shown D is aligned in the direction of apparent wind v_a and L is orthogonal to it. The angle of attack can be defined as the sum of the pitch angle α_u determined with respect to the horizon and the relative wind orientation α_w . The apparent wind velocity \vec{v}_a is defined by:

$$\vec{v}_a = \vec{v}_w - \vec{v}_k \quad (2)$$

where \vec{v}_k is the translation velocity of the flying device and \vec{v}_w is the wind speed. Several wing configurations can be studied. Notice that, the absence of an actuator that links the drone to the wing, leads to a fixed relative angle, α_u can be expressed as:

$$\alpha_u = \phi + \alpha_D \quad (3)$$

where α_D is a fixed design value. The configurations of the system for two different values of α_d are presented in Fig. 5.



Fig. 5 Examples of fixed configuration between the wing and the drone. Left figure is the system used in this paper for the experimentation that correspond to $\alpha_D = 0$, and right figure correspond to another configuration where $\alpha_D = \pi/2$.

In this present study, only the system motion in the vertical plane is considered, assuming that the system is aligned to the main wind direction and it only experiences small variations in the third dimension. It is also assumed that the tether of length r forms a straight line. This assumption is acceptable for a taut tether of small length since in this case the linear mass is negligible. Otherwise, a tether model should be added in order to take into account its influence. The

tension in the tether is T_T . The tether has an elevation angle β with respect to the horizontal plane. The drone has an inclination angle ϕ with respect to the vertical axis and produces a thrust force T_D . All these variables are represented on Fig. 4. The combined mass of all airborne system components is denoted by M_M . For the drone attached to the rigid wing, the following equation is used to express its closed-loop dynamics model :

$$\dot{T}_D = \frac{1}{\tau_{T_D}} (T_D^d - T_D), \quad \dot{\phi} = \frac{1}{\tau_{\phi}} (\phi^d - \phi) \quad (4)$$

where T_D^d and ϕ^d are the desired thrust and inclination angle sent to the drone, and τ_{T_D} and τ_{ϕ} are the time constants of the first order systems in eq. 14.

The fundamental principle of dynamics is applied to establish a dynamical model of the flying device of Fig. 4. Considering the system's two degrees of freedom, r and β , translation velocity of the flying device \vec{v}_k can be decomposed into a radial velocity component $v_{k,r} = \dot{r}$ and a tangential velocity component $v_{k,\tau} = r\dot{\beta}$. As done in [13], differentiation of \vec{v}_k with respect to time yields a radial acceleration component and a tangential acceleration component:

$$\frac{dv_{k,r}}{dt} = \ddot{r} - r\dot{\beta}^2, \quad \frac{dv_{k,\tau}}{dt} = r\ddot{\beta} + 2\dot{r}\dot{\beta} \quad (5)$$

As illustrated on Fig. 4, the resultant forces F_r and F_τ are respectively the radial and tangential force components according to the polar coordinate system (r, β) .

$$F_r = -T + L \sin(\beta - \alpha_w) + D \cos(\beta - \alpha_w) - P \sin \beta - T_D \sin(\phi - \beta) \quad (6)$$

$$F_\tau = L \cos(\beta - \alpha_w) - D \sin(\beta - \alpha_w) - P \cos \beta + T_D \cos(\phi - \beta) \quad (7)$$

The tether tension can be calculated using:

$$T_T = T + M_D \ddot{r} \quad (8)$$

It corresponds to the desired tension in the tether plus the force coming from the acceleration of the drum. The system's weight is P . α_w is the angle that the apparent wind velocity forms with the horizontal. It can be calculated with the formula of [12]:

$$\alpha_w = \arctan \frac{r \cos(\beta) \dot{\beta} + \dot{r} \sin(\beta)}{v_w + r \sin(\beta) \dot{\beta} - \dot{r} \cos(\beta)} \quad (9)$$

The dynamic model can then be derived in 2D polar coordinates:

$$\ddot{r} = \frac{1}{M_M + M_D} \left[r\dot{\beta}^2 M_M + F_r \right] \quad (10)$$

$$\ddot{\beta} = \frac{1}{r} \left[-2\dot{\beta}\dot{r} + \frac{F_\tau}{M_M} \right] \quad (11)$$

where $M_D = \frac{I}{R_d^2}$ is expressed in function of the inertia moment of the on-ground generator I and its radius R_d . One can add a third equation, that is the dynamical equation of the on-ground generator traction force:

$$\dot{T} = \frac{1}{\tau_T} (u_r^d - T) \quad (12)$$

where u_r^d is the desired traction force, used to control tether length r , T is the effective torque of the drum divided by its radius R_d and τ_T is the time constant of the dynamic system considered as a first order system.

To summarize, the overall nonlinear model of the system can be written as:

$$\begin{aligned} \ddot{r} &= \frac{1}{M_M + M_D} \left[r\dot{\beta}^2 M_M - T - P \sin(\beta) + u_{T_0} + L \sin(\beta - \alpha_w) \right. \\ &\quad \left. + D \cos(\beta - \alpha_w) \right] \\ \ddot{\beta} &= \frac{1}{r} \left[-2\dot{\beta}\dot{r} + \frac{1}{M_M} (-P \cos(\beta) + u_\beta + L \cos(\beta - \alpha_w) - D \sin(\beta - \alpha_w)) \right] \\ \dot{T} &= \frac{1}{\tau_T} (u_r^d - T) \\ u_{T_0} &= -T_D \sin(\phi - \beta) \\ u_\beta &= T_D \cos(\phi - \beta) \\ \dot{T}_D &= \frac{1}{\tau_{T_D}} (T_D^d - T_D) \\ \dot{\phi} &= \frac{1}{\tau_\phi} (\phi^d - \phi) \end{aligned} \quad (13)$$

Drone inputs are computed from u_{T_0} and u_β that are used to control the elevation angle β and the tether tension T_T , respectively. Note that in eq. 14 there are two actuators, T and u_{T_0} in order to control two variables: r and T_T . The winch torque T , the faster and more precise actuator, is then used to control r , that is the more critical variable of the system than tether tension T_T , that has just to be maintained positive and thus is controlled with the thrust generated by the drone.

III. Methodology

A. Controller Design

In this section, we propose a nonlinear controller that provides the control values u_r^d , u_{T_0} and u_β . Based on the flatness principle, at the first stage, an output-feedback linearization control is determined. The aim of this stage is to transform the nonlinear tracking problem to a simple linear stabilizing problem. For sake of control design and without any loss of generality, the lift and drag forces can be considered as disturbances. Thus, the control law has to ensure the desired performance while compensate the effect of the poorly-known lift and drag forces. Then, at the second stage, an intermediate linear control law is computed to ensure the asymptotic stability of the tracking error.

The considered external and internal variables of this system are defined as follows:

$$\text{Input vector } u = \begin{pmatrix} u_r^d & u_\beta \end{pmatrix}^T, \text{ Output vector } y = \begin{pmatrix} r & \beta \end{pmatrix}^T, \text{ State vector } x = \begin{pmatrix} r & \dot{r} & \beta & \dot{\beta} \end{pmatrix}^T$$

The state variables r , \dot{r} , β and $\dot{\beta}$ can be measured using sensors as explained in subsection III.C. For the control design, and since the dynamics of the current loop of the winch is very faster with respect to all other electromechanical loops of the system, we can neglect it and consider simply $T = u_r^d$. Then, the following simplified model is obtained from eq. 14:

$$\dot{x} = \begin{pmatrix} \dot{r} \\ \frac{1}{M_M + M_D} \left[r \dot{\beta}^2 M_M + (-u_r^d - P \sin(\beta) + u_{T_0}) \right] \\ \dot{\beta} \\ \frac{1}{r} \left[-2\dot{\beta} \dot{r} + \frac{1}{M_M} (-P \cos(\beta) + u_\beta) \right] \end{pmatrix} \quad (14)$$

As it can be clearly shown, the relative degree of the system is 2. This corresponds to the number of times one needs to differentiate the output y before the input u appears explicitly (see eq. 16).

$$y = \begin{pmatrix} 1 & 0 & 0 & 0 \\ 0 & 0 & 1 & 0 \end{pmatrix} x, \quad \dot{y} = \begin{pmatrix} \dot{r} \\ \dot{\beta} \end{pmatrix} = \begin{pmatrix} 0 & 1 & 0 & 0 \\ 0 & 0 & 0 & 1 \end{pmatrix} x \quad (15)$$

$$\ddot{y} = \underbrace{\begin{pmatrix} \frac{1}{M_M + M_D} \left[r \dot{\beta}^2 M_M - P \sin(\beta) + u_{T_0} \right] \\ \frac{1}{r} \left[-2\dot{\beta} \dot{r} - \frac{P}{M_M} \cos(\beta) \right] \end{pmatrix}}_{b(x)} + \underbrace{\begin{pmatrix} -\frac{1}{M_M + M_D} & 0 \\ 0 & \frac{1}{M_M} \frac{1}{r} \end{pmatrix}}_{A(x)} \underbrace{\begin{pmatrix} u_r^d \\ u_\beta \end{pmatrix}}_u \quad (16)$$

From eq. 16, one gets that \ddot{y} is affine with respect to the input u . Under the hypothesis that the matrix $A(x)$ is invertible, which is the case in our operating range, the nonlinear control law defined by:

$$u = A^{-1}(x)(v - b(x)) \quad (17)$$

reduces the nonlinear system's dynamics to the dynamics of a double integrator $\ddot{y} = v$ with v is the linear intermediate control law. Thus, to ensure the stability of the tracking error, we propose to use a multi-variable proportional-integral-

derivative controller, $v = \begin{pmatrix} v_r \\ v_\beta \end{pmatrix}$ with

$$v_r = \alpha_{r-1} \int_0^t e_r(\tau) d\tau + \alpha_{r0} e_r + \alpha_{r1} \dot{e}_r + \ddot{y}_r^d \quad (18)$$

$$v_\beta = \alpha_{\beta-1} \int_0^t e_\beta(\tau) d\tau + \alpha_{\beta0} e_\beta + \alpha_{\beta1} \dot{e}_\beta + \ddot{y}_\beta^d \quad (19)$$

where $y^d = [y_r^d \ y_\beta^d]^T$ is the vector of the desired setpoints, $e = (y^d - y)$ is the vector of tracking error. Note that, the integral term is added in order to improve the robustness of the controller. That is, to be able to reject disturbances and to compensate the modelling error, for instance the non considered lift and drag forces. The Integral of the Time weighted Absolute Error (ITAE) performance index is used in order to tune the controller parameters. It allows to specify the dynamic response with relatively small overshoot and relatively little oscillation. The characteristic polynomial is

$$P(s) = s^3 + 1.783w_n s^2 + 2.172w_n^2 s + w_n^3 \quad (20)$$

with w_n the natural frequency of the closed-loop system. Note that, by this choice one can get a stable linear tracking error with a desired converging rate. To compensate oscillations of the reel-in and reel-out speeds \dot{r} due to error on the simplified model, the derivative coefficient is increased by 20%, giving $\alpha_{r1} = 2.1396w_n$. This value has been found on the test bench thanks to experimentation. For the design of u_{T_0} , we have chosen to use an open loop control with a simple feedforward compensation of the weight:

$$u_{T_0} = T_0^d + P \sin(\beta) \quad (21)$$

In an equilibrium position, u_{T_0} has to compensate the weight and the desired tension in the tether. By decomposing the action of the drone into a radial component and tangential one, it is important to mention that the radial part u_{T_0} enters directly in concurrence with the winch's torque that controls r . This simple law allows to obtain a thrust force that will

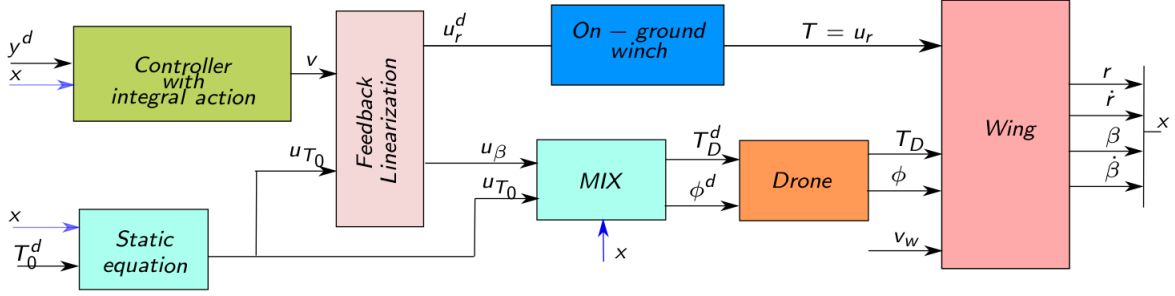


Fig. 6 Block diagram of the control strategy.

smoothly maintain the minimum desired tension in the tether without perturbing the control law on r , as long as the thrust is well calibrated. This calibration is detailed in III.C.6. This choice has been done in order to study properly the control law on r , nevertheless, a more advanced control law can be designed for this part in order to track faster and more precisely the tether tension.

The block diagram on Fig. 6 shows the different stages to be carried out to provide the control action. The "Drone" block corresponds to the drone that has its own internal control loops and can be modelled by the simplified model of eq. 14. The "Wing" block corresponds to the whole flying part that can be modelled by eq. 11, eq. 10, eq. 1 and data from Fig. 3.

The block MIX allows to transform the input u_β and u_{T_0} in input command for the drone, T_D^d and ϕ^d . A simple equation is used :

$$\begin{aligned} T_D^d &= \sqrt{u_{T_0}^2 + u_\beta^2} \\ \phi^d &= \text{atan}\left(-\frac{u_{T_0}}{u_\beta}\right) + \beta \end{aligned} \quad (22)$$

However this transformation can be improved to deal with the influence of aerodynamics forces for example. To compensate the delay due to the response time of drone actuators, a transformation is also made in this block MIX :

$$T_{D\text{compensated}} = T_D^d + \tau_{T_D} \dot{T}_D^d \quad (23)$$

$$\phi_{\text{compensated}} = \phi^d + \tau_\phi \dot{\phi}^d \quad (24)$$

where τ_{T_D} and τ_ϕ are the identified time response of the drone actuators. A prediction using an Euler model is done. To obtain \dot{T}_D^d and $\dot{\phi}^d$ a finite difference approximations method is used.

B. Experimental 3D Implementation

As mentioned in the previous sections, the model and the designed control law are in the plane (2D) and only two inputs of the drone are considered: T_D and ϕ . However, in the space (3D), azimuth angle of the system η , as well as roll angle θ and yaw angle ψ of the drone has to be controlled (see Fig. 7). An additional control law for η and ψ angles has been designed. In order to stay as much as possible equivalent to the 2D problem, the yaw is chosen such that the drone is always pointing to the ground station. Notice that, the drone has its internal control loop that regulates the yaw angle to its desired value $\psi_d = \pi + \eta$. To regulate azimuth angle η , the roll angle θ that is also locally controlled by the drone is used. This angle η is set in a way to have the system aligned with the wind, or in particular in our indoor situation aligned with x axis. The same approach is employed for elevation angle β control law detailed in section III.A:

$$\ddot{\eta} = \frac{1}{r}(-2\dot{\eta}\dot{r} + \frac{1}{M_M}u_\eta) \quad (25)$$

$$u_\eta = M_M r(v_\eta + \frac{2\dot{\eta}\dot{r}}{r}) \quad (26)$$

$$v_\eta = \alpha_{\eta-1} \int_0^t e_\eta(\tau) d\tau + \alpha_{\eta 0} e_\eta + \alpha_{\eta 1} \dot{e}_\eta + \ddot{\eta}_r^d \quad (27)$$

$$e_\eta = \eta_{ref} - \eta \quad (28)$$

In eq. 26 the input command u_η is obtain thanks to a feedback linearization method on the dynamical model of η given in eq. 25. Then a linear command v_η is design in the same way than v_β and the coefficient are chosen thanks to the ITAE criteria.

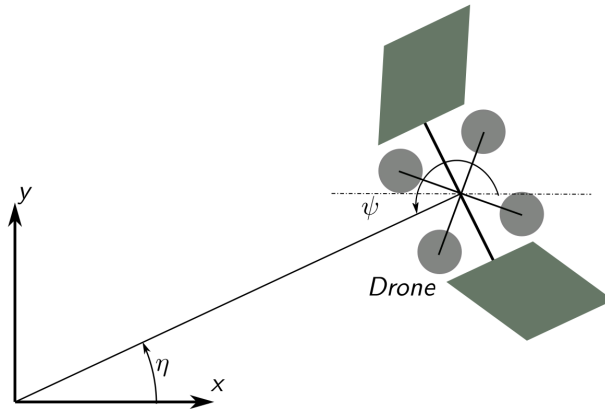


Fig. 7 Top view of the system.

C. Experimental benchmark

The experimental benchmark is composed of wings attached to a drone and linked together to an on-ground winch with a tether. A motion capture system tracks the drone position and sends it to an on-ground computer that controls the winch and the drone. Figure 8 shows the global architecture of the system.

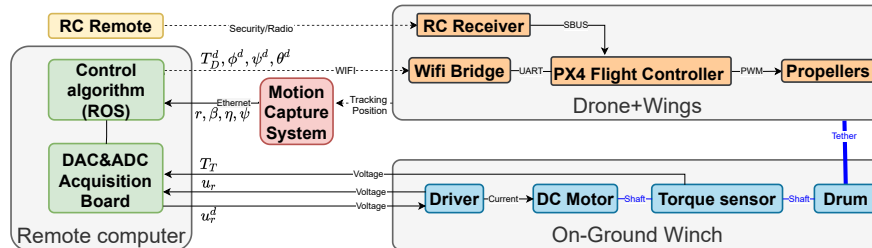


Fig. 8 Global architecture of the benchmark.

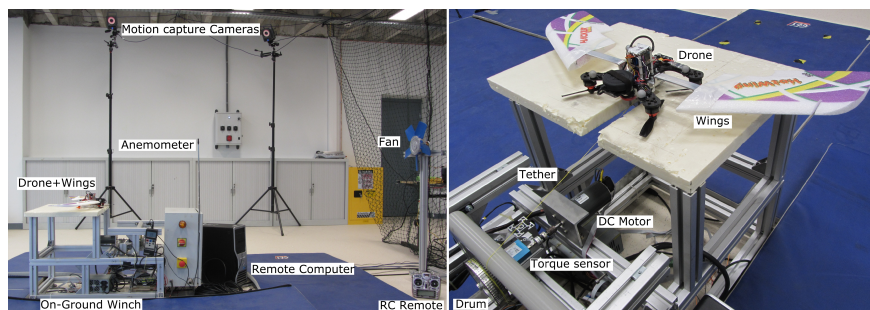


Fig. 9 The different components of the benchmark.

1. Drone

The drone is composed of 4 NOVA RM2206-KV2300 motors with 5046BN propellers, driven by 30A Electronic Speed Controllers (ESC). A 3S 1300mAh LiPo battery ensure the power supply of the drone. The flight controller is a STM32 based KAKUTE F7 from Holybro, running the PX4 autopilot. It communicates with through a Wi-Fi/serial bridge made with an ESP32 micro-controller. PX4 Autopilot uses its embedded inner loop to control the attitude of the drone, based on an embedded estimator that uses IMU and a measurement of the position that comes from the motion capture system[‡]. Setpoints sent to the drone through a mavlink protocol are the global thrust and Euler angles roll, pitch and yaws. Propellers are chosen to point downwards in order to have a center of mass as close as possible of the bridle point of the tether. This reduces the amplitude of the disturbance torques induced by the pulling force of the tether on the drone. Wings are Hotwing 500 model, made from polystyrene and fabricated by Hacker Model. Its area of $0.09m^2$ allows one to potentially generate a rated power around 300W. A remote controller communicates directly with the flight controller through a FrSky radio protocol to ensure emergency stop functions.

[‡]<https://docs.px4.io/master>

2. On-ground Winch

On-ground winch is actuated with a 100W Maxon 2260L DC-Motor driven by a four-quadrants amplifier Maxon ADS 50/10 that controls its current. The drum of 5cm radius is linked to that motor through a Kistler 4502a rotating torque sensor that provides an accurate measure of the tether tension T_T . Current setpoint and current torque measurement are connected to the remote computer with a DAC PCI DAS1200 board from Measurement Computing.

3. Motion capture system

Motion capture system is a set of 9 Vicon T40s cameras that tracks a pattern of reflectors fixed to the drone and give its position and orientation. It is run on a dedicated computer that uses the Tracker Vicon software and is able to communicate with the remote computer through the VRPN protocol. From Cartesian position of the drone provided by the motion capture system, the algorithm computes its spherical coordinates r , β and η (see eq. 29).

$$\begin{aligned} r &= \sqrt{x^2 + y^2 + z^2}, & \dot{r} &= \frac{\dot{x}x + \dot{y}y + \dot{z}z}{r}, & \beta &= \operatorname{atan}\left(\frac{z}{\sqrt{x^2 + y^2}}\right) \\ \eta &= \operatorname{atan}\left(\frac{y}{x}\right), & \dot{\eta} &= \frac{\dot{y}x - y\dot{x}}{x^2 + y^2}, & \dot{\beta} &= \frac{\dot{z}\sqrt{x^2 + y^2} - z\frac{(\dot{x}x + \dot{y}y)}{\sqrt{x^2 + y^2}}}{r^2} \end{aligned} \quad (29)$$

Note that in an outdoor experimentation, where the use of a motion capture system is no longer possible, one has to use GPS position to provide the coordinates of the drone with a much lower accuracy and frequency. Consequently, in order to measure an accurate value of tether length r , the use of an incremental coder fixed on the DC motor of the winch would be a better strategy.

4. Remote computer

The on-ground remote computer is an Ubuntu desktop computer based on an Intel Xeon 2.53Ghz processor. The control algorithm is implemented within the ROS middleware and run at a frequency of 100Hz. The interface with the motion capture system use the `vrpn_client_ros` node [§] and the communication with the drone is performed through the `mavros` package ¶.

5. Wind disturbance

In order to produce a wind disturbance on the system, we used a 38cm fan positioned at $-2.1m$ along x axis and $67.5cm$ along z axis. A hot wire anemometer provides a local mean measurement of the produced wind at the same altitude as the fan and $-0.38m$ along x axis. As it leads to a highly perturbed airflow, including rotating movement

[§]<http://wiki.ros.org>

[¶]<http://wiki.ros.org/mavros>

induced by the rotation of the fan, the obtained measurement is used only to have a relative quantification of the mean magnitude of the disturbance, and thus only to compare one situation to another. For example in section IV, a scenario with no wind disturbance is compared to a scenario with a wind disturbance, which is in average around $2m/s$.

6. Parameter identification

All necessary identified physical parameters of the system are gathered into Table 1. To identify the time response τ_ϕ of the closed loop of the inclination angle ϕ , a first order model (in blue) is fitted on experimental data (in red) on Fig. 10. A fit of 33.62% is obtained for a value of $\tau_\phi = 0.194s$. We also identified with the same method the time constant of a first order model for the current loop of the DC winch's motor. This loop is fast enough to be considered as instantaneous with regard to the whole system dynamics. As it is difficult to have an accurate measure of the thrust force of the drone, we estimated its first order model by seeking the time response of the position of the drone at the first take-off, which corresponds to a situation that is close to a step response. On the other hand, a hover is performed on the drone with no tether to calibrate the thrust that compensate the mass of the system.

Table 1 Physical Parameters

Symbol	Name	Value
M_M	Mass of airborne subsystem	0.774 kg
M_D	Ground station rotor mass	0.0481 kg
S	Wing area	$0.09 m^2$
α_D	Wing configuration angle	0 deg
ρ	Air density	$1.225 kg/m^3$
τ_T	Time constant of motor current loop	0.02 s
τ_{T_D}	Time constant of drone thrust loop	0.085 s
τ_ϕ	Time constant of drone inclination loop	0.194 s
$u_{r\ min}$	Minimum tension in the winch	0 N
$u_{r\ max}$	Maximum tension in the winch	8 N
$T_{D\ min}$	Minimum drone's thrust	0 N
$T_{D\ max}$	Maximum drone's thrust	17.7 N
$\phi_{\ min}$	Minimum drone's inclination angle	-50 deg
$\phi_{\ max}$	Maximum drone's inclination angle	50 deg

Note that parameters S , α_D , τ_T , ρ , as well as aerodynamic parameters of the wing (Fig. 3) are not used to the experimental implementation but only for simulation purpose.

D. Scenario for Validation

To validate the performance of the proposed control strategy, it is tested on a scenario including a take-off and a landing, first in simulation and then in experiment. During all the scenario the desired tension in the tether T_0^d is set to 1.5N and the desired azimuth angle η_{ref} is equal to 0° . The scenario is the following:

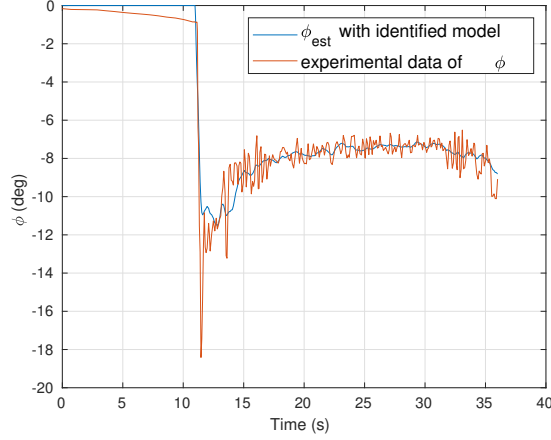


Fig. 10 Identification of τ_ϕ

- Initial position: The system starts from its initial position at $r_0 = 0.4m$, $\beta_0 = 40^\circ$, $T_{D_0} = 0N$ and $\phi_0 = 0$.
- Take-off phase: At $t = 0$ s the reference signal r_d goes from r_0 to $r_f = 1.2m$ with a ramp rate of $0.08m/s$, and the desired elevation angle β_d goes from β_0 to $\beta_f = 45^\circ$ with a ramp rate of $0.5^\circ/s$.
- Landing phase: At $t = 25$ s the reference signal r_d goes from r_f to r_0 with a ramp rate of $0.08m/s$, and the desired elevation angle β_d goes from β_f to β_0 with a ramp rate of $0.5^\circ/s$.
- End of the scenario : Once the system is landed, the drone is back to its initial position and ready to start a new cycle.

Table 2 Parameters of the controller

Symbol	Name	Value
ω_{nr}	Natural frequency for the r loop	5 rad/s
$\omega_{n\beta}$	Natural frequency for β loop	3 rad/s
$\omega_{n\eta}$	Natural frequency for η loop	3 rad/s

The scenario is done firstly with no wind disturbance and a secondly with wind disturbances around $2m/s$. The value of the parameters of the controller are given in Table 2, the value of w_{nr} is higher than $w_{n\beta}$ and $w_{n\eta}$ since it is assume that the control loop in r is faster than in β and η . Results are presented and discussed in the following section.

IV. Results and discussion

Experimental results are presented in Figs. 11 to 16, the left sides it corresponds to the results obtained in the no wind disturbance scenario $v = 0m/s$ and the right side shows the obtained results in the presence of wind disturbance, $v = 2m/s$.

In Fig. 11, the evolution of the tether length r , in blue, is compared to the desired length in red. In both scenario, it follows well the reference. The command input u_r is also presented. It shows that it never attains the saturation values,

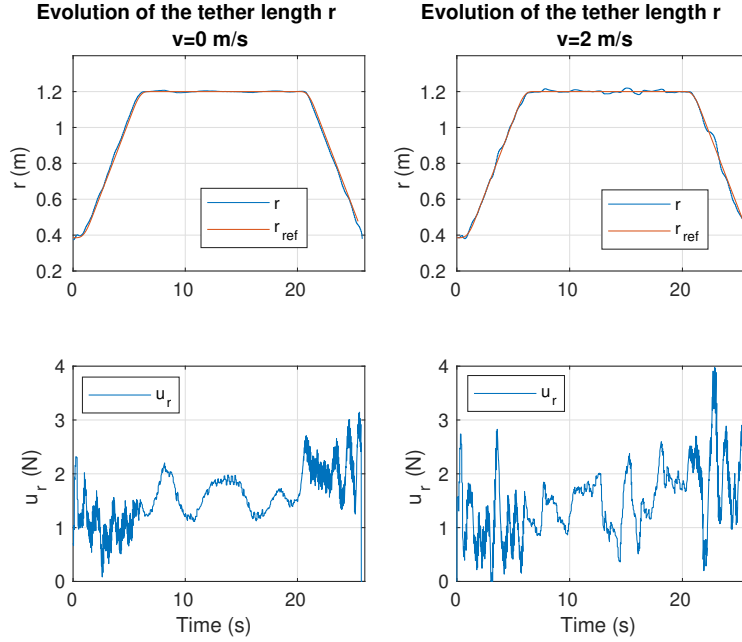


Fig. 11 Evolution of the tether’s length r compared to its desired value and its control input u_r , the desired traction force sent to the winch.

$u_{r_{max}} = 8N$. The evolution of the elevation angle β is represented on Fig. 12 as well as its command input u_β . This

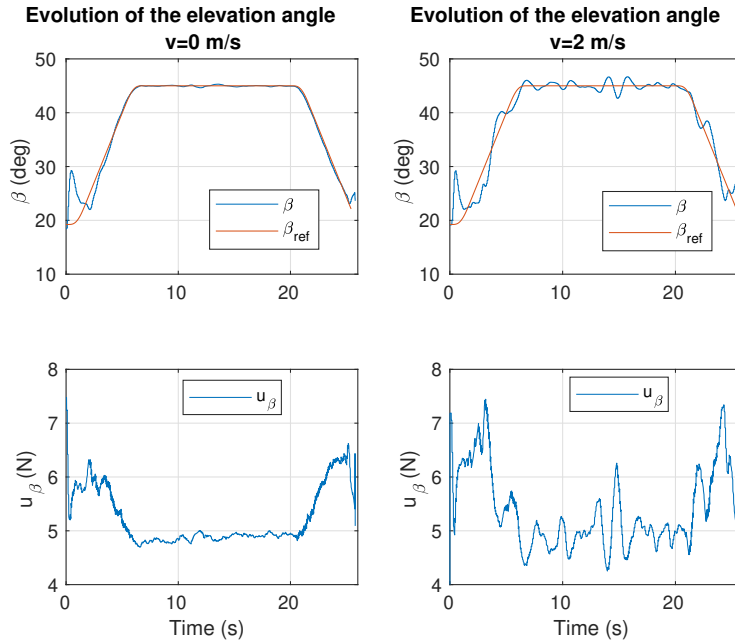


Fig. 12 Evolution of the elevation angle β compared to its desired value and its control input u_β , the lateral desired force of the drone.

state variable is more disturbed with wind but still follows the reference trajectory. A jump can be seen at the beginning

of the take-off, it is partially due to the ground effect.

The last state variable, the azimuth angle η is shown in Fig. 13. Some oscillations around the reference value 0° at the beginning can be observed during the transient period and then η converges towards its reference value. Oscillations are less attenuated in presence of wind. This is principally due to the turbulent nature of the wind generated by the fan. For a wind superior to $3m/s$ the system is not able to stabilize the azimuth angle.

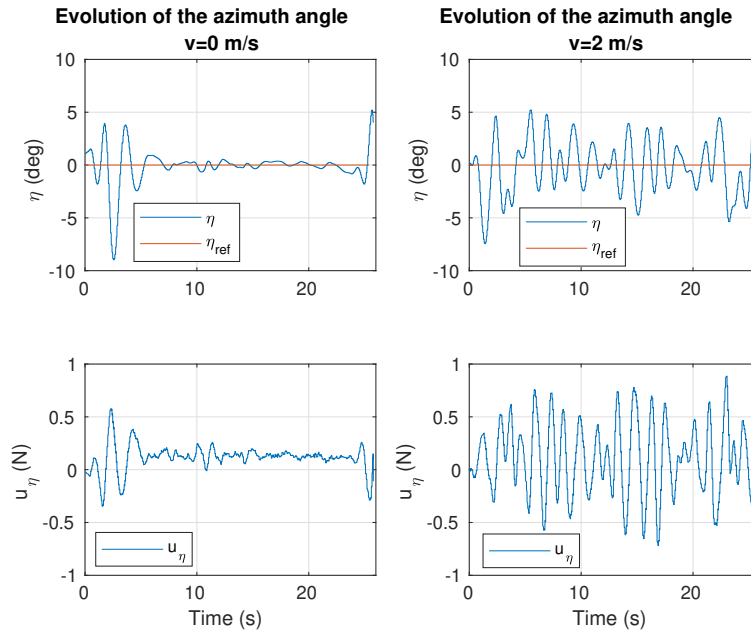


Fig. 13 Evolution of the azimuth angle η compared to its desired value and its control input u_η , the peripheral desired force of the drone using its roll command.

An important point is that the tether has to be always taut, meaning the tether tension T_T is above $0N$. This tension is shown on Fig. 14 where there is in blue the desired tension T_0 and in red the real tension T_T . The tether tension never goes below $0.7N$ for the no wind scenario and is always above $0.2N$ in the scenario with a wind around $2m/s$ and is in average around the desired value for both scenario. Its command u_{T_0} shows that even if the control law is in open loop, the command takes into account the influence of the weight and elevation angle β . However, the open loop doesn't allow to reject disturbances and modeling errors. In presence of wind, the high frequency aerodynamic forces disturbances can be seen. On Fig. 16, the trajectory of the system during the scenario is represented in 2D. In black, this is the desired trajectory, in red the one described by the system during the take-off and in blue during the landing. The black rectangle corresponds to the on-ground station and in light blue, the tether is represented. The system is represented in pink on this figure at one position of the overall trajectory. The drone stays near the desired trajectory and never get in a critical zone. Since the objective is to attain a desired position and not to follow perfectly the entire trajectory, this result is satisfying. The higher the wind speed is the more the trajectory is disturbed but in its overall trajectory it follows well the reference and it never gets in a critical zone where the system could crash. At the beginning of the take-off phase, T_T

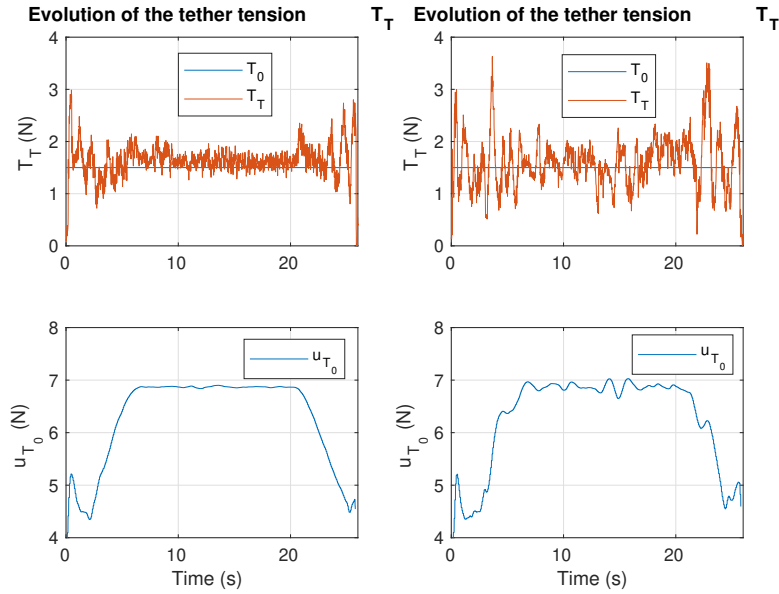


Fig. 14 Evolution of the tether tension T_T compared to its desired value and its control input u_{T_0} , the radial desired force of the drone.

and β take time to stabilize at the desired value. This is due to ground effects which add a force to the thrust of the drone, so the behavior of the drone doesn't correspond to the model. For the tether length, no such overshoot is observed. This is thanks to the choice of the actuator: the winch commands the tether length and this actuator is very accurate, that allows an efficient control of the tether length. The drone inputs ϕ_{ref} and ϕ , the inclination angle measured by the

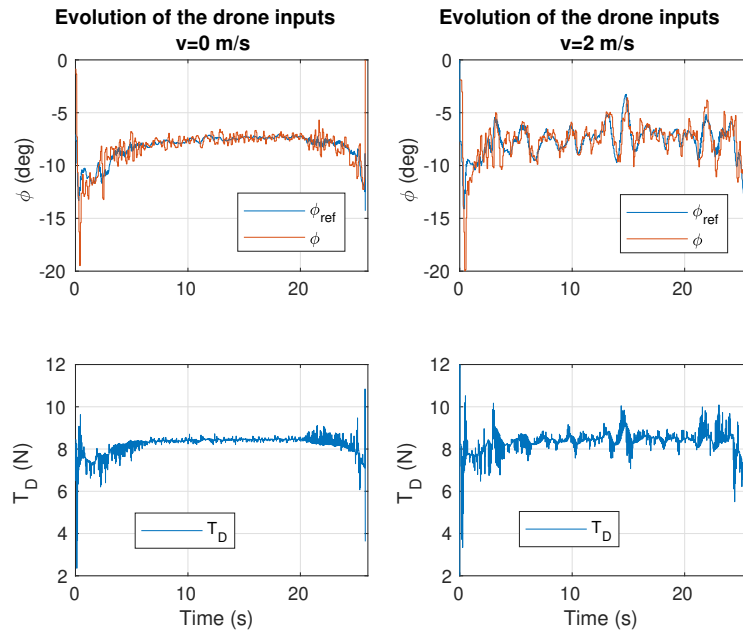


Fig. 15 Evolution of drone inputs ϕ and T_D .

motion capture, and T_D , the thrust, are shown on Fig. 15. The inclination angle stabilize itself around $-7deg$ and the thrust is around $8N$. On the inclination angle, the influence of the delay compensation is efficient. The two signals ϕ_{ref} and ϕ are well synchronized.

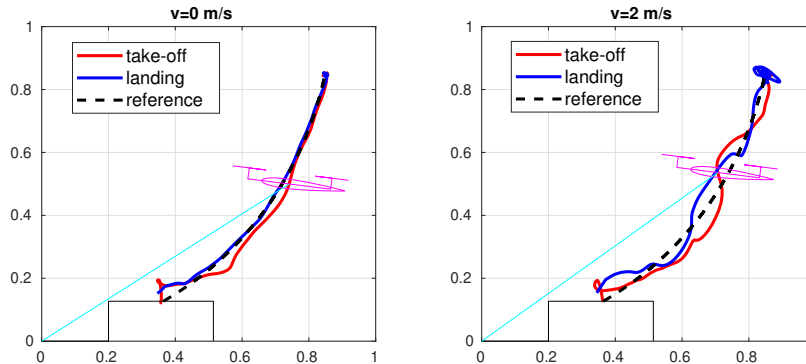


Fig. 16 Trajectory of the system.

V. Conclusion

The main objective is to design a controller to perform a take-off and a landing. The obtained results have shown that the objective is attained and the choice of the actuators for controlling the systems states is relevant. In this work, the configuration $\alpha_D = 0$ has been studied but the work can be extended to other configurations. A choice have been made to perform the modeling in the plane (2D) and then extend the control law to 3D space. However, the modelling can also be done directly in 3D, if the variations of η are taken into account. Keeping the same feedback linearization method stage, the next step is to consider the aerodynamics forces in the MIX block. Elevators and rudders can be added and controlled in this block together with the drone control variables in order to maintain performances for a wide range of wind conditions. A control law in closed loop for the tether tension could be designed. Finally as the experiments have shown that the ground-effect was not negligible at the beginning of the take-off and the end of the landing phases, it could be interesting to integrate this effect in the modelling and control design.

Acknowledgment

The authors would like to thank the technical staff of Gipsa-lab, and particularly Remy Jaccaz and Sylvain Geranton who provided an important technical support in the construction of the experimental set-up. The equipment used in the paperr was partially funded by Equipex Robotex (ANR-10-EQPX-44-01).

References

- [1] Chris Vermillion, Mitchell Cobb, Lorenzo Fagiano, Rachel Leuthold, Moritz Diehl, Roy S. Smith, Tony A. Wood, Sebastian Rapp, Roland Schmehl, David Olinger, and Michael Demetriou. “Electricity in the air: Insights from two decades of

- advanced control research and experimental flight testing of airborne wind energy systems”. In: *Annual Reviews in Control* (2021). ISSN: 1367-5788. DOI: <https://doi.org/10.1016/j.arcontrol.2021.03.002>. URL: <https://www.sciencedirect.com/science/article/pii/S1367578821000109>.
- [2] Roland Schmehl, ed. *Airborne Wind Energy Conference*. Delft, The Netherlands: Delft University of Technology, 2015, p. 9. ISBN: 978-94-6186-486-4. DOI: [10.4233/uuid:7df59b79-2c6b-4e30-bd58-8454f493bb09](https://doi.org/10.4233/uuid:7df59b79-2c6b-4e30-bd58-8454f493bb09).
- [3] Mario Zanon, Sébastien Gros, and Moritz Diehl. “Rotational start-up of tethered airplanes based on nonlinear MPC and MHE”. In: *2013 European Control Conference (ECC)*. IEEE. Zurich, Switzerland, 2013, pp. 1023–1028. DOI: [10.23919/ECC.2013.6669743](https://doi.org/10.23919/ECC.2013.6669743).
- [4] Burkhard Rieck, Maximilian Ranneberg, Ashwin Candade, Alexander Bormann, and Stefan Skutnik. “Comparison of Launching & Landing Approaches”. In: *Book of Abstracts of the International Airborne Wind Energy Conference (AWEC 2017)*. Ed. by Moritz Diehl, Rachel Leuthold, and Roland Schmehl. Freiburg, Germany: University of Freiburg | Delft University of Technology, Oct. 5–6, 2017, pp. 121–123. DOI: [10.6094/UNIFR/12994](https://doi.org/10.6094/UNIFR/12994).
- [5] Lorenzo Fagiano and Stephan Schnez. “On the take-off of airborne wind energy systems based on rigid wings”. In: *Renewable energy* 107 (2017), pp. 473–488. DOI: [10.1016/j.renene.2017.02.023](https://doi.org/10.1016/j.renene.2017.02.023).
- [6] Massimo Canale, Lorenzo Fagiano, and Mario Milanese. “KiteGen: A revolution in wind energy generation”. In: *Energy* 34.3 (2009), pp. 355–361. DOI: [10.1016/j.energy.2008.10.003](https://doi.org/10.1016/j.energy.2008.10.003).
- [7] Aldo U Zraggen, Lorenzo Fagiano, and Manfred Morari. “Automatic retraction and full-cycle operation for a class of airborne wind energy generators”. In: *IEEE Transactions on Control Systems Technology* 24.2 (2016), pp. 594–608. DOI: [10.1109/TCST.2015.2452230](https://doi.org/10.1109/TCST.2015.2452230).
- [8] Florian Bauer, Christoph M Hackl, Keyue Smedley, and Ralph M Kennel. “Multicopter-based launching and landing of lift power kites”. In: *Airborne Wind Energy*. Springer, 2018, pp. 463–489. DOI: [10.1007/978-981-10-1947-0_19](https://doi.org/10.1007/978-981-10-1947-0_19).
- [9] Sebastian Rapp and Roland Schmehl. “Vertical Takeoff and Landing of Flexible Wing Kite Power Systems”. In: *Journal of Guidance, Control, and Dynamics* 41.11 (2018), pp. 2386–2400. DOI: [10.2514/1.G003535](https://doi.org/10.2514/1.G003535).
- [10] Audrey Schanen, Jonathan Dumon, Nacim Meslem, and Ahmad Hably. “Take-off and landing of an AWE system using a multicopter”. In: *2020 American Control Conference (ACC)*. IEEE. 2020, pp. 3846–3851. DOI: [10.23919/ACC45564.2020.9148035](https://doi.org/10.23919/ACC45564.2020.9148035).
- [11] Rogelio Lozano Jr, Mazen Alamir, Jonathan Dumon, and Ahmad Hably. “Control of a wind power system based on a tethered wing”. In: *IFAC Workshop on Embedded Guidance, Navigation and Control in Aerospace (EGNCA 2012)*. Bangalore, India, Feb. 2012. DOI: [10.3182/20120213-3-IN-4034.00027](https://doi.org/10.3182/20120213-3-IN-4034.00027).
- [12] Rogelio Lozano, Jonathan Dumon, Ahmad Hably, and Mazen Alamir. “Energy production control of an experimental kite system in presence of wind gusts”. In: *2013 IEEE/RSJ International Conference on Intelligent Robots and Systems*. IEEE. 2013, pp. 2452–2459. DOI: [10.1109/IROS.2013.6696701](https://doi.org/10.1109/IROS.2013.6696701).

- [13] Ahmad Hably, Jonathan Dumon, Garrett Smith, and Pascal Bellemain. *Control of a Magnus Effect-Based Airborne Wind Energy System*. Ed. by Roland Schmehl. Singapore: Springer Singapore, 2018, pp. 277–301. doi: [10.1016/j.ifacol.2017.08.2205](https://doi.org/10.1016/j.ifacol.2017.08.2205).